Electronic Supplementary Material (ESI) for Journal of Materials Chemistry A.
This journal is © The Royal Society of Chemistry 2024

# Electronic Supplementary Information for

## Synergistic Design of g-$C_3N_4$-Supported CNTs: Experimental and DFT Insights for Enhanced Electrochemical Performance in Flexible Li-S batteries

Vijay K. Tomer[a,*], Rameshwar L. Kumawat[b], Otavio Augusto Titton Dias[a], Ritu Malik[a,*], George C. Schatz[b], Mohini Sain[a]

[a] Department of Mechanical & Industrial Engineering, University of Toronto, Canada

[b] Department of Chemistry, Northwestern University, Illinois, USA

***Corresponding author: vj.kumar@utoronto.ca; ritu.kumar@utoronto.ca**

**Gibbs Free Energy of Sulfur Reduction Reaction (SRR):**

The reaction Gibbs free energy of $S_8$ and $Li_2S_n$ on g-$C_3N_4$ and g-$C_3N_4$-CNT composite surfaces were calculated by using the following equation:

$$\Delta G = \Delta E_{dft} - (\Delta ZPE + T\Delta S) \qquad (1)$$

where $\Delta E_{dft}$ represents the difference between products and reactants computed by DFT calculation, $\Delta ZPE$ and $T\Delta S$ are the difference of the zero-point energy (ZPE), and entropic contribution, respectively. The $\Delta E_{dft}$ is obtained from the corresponding VASP computation, while the ZPE, enthalpy and entropy contributions are computed from vibrational frequency calculations and using the Vaspkit tool at a temperature of 300 K.

In the discharging process of Li−S batteries, the overall sulfur reduction reaction (SRR) involving an $S_8$ molecule is a 16-electron process, resulting in the generation of $8Li_2S$ molecules:

$$S_8 + 16Li^+ + 16e^- \rightarrow 8Li_2S$$

The individual steps for the formation of one $Li_2S$ molecule are described as follows, where * denotes an active site on the catalytic surface:

$$*S_8 + 2Li^+ + 2e^- \rightarrow *Li_2S_8 \qquad \text{(SRR1)}$$

$$*Li_2S_8 \rightarrow *Li_2S_6 + (1/4)S_8 \qquad \text{(SRR2)}$$

$$*Li_2S_6 \rightarrow *Li_2S_4 + (1/4)S_8 \qquad \text{(SRR3)}$$

$$*Li_2S_4 \rightarrow *Li_2S_2 + (1/4)S_8 \qquad \text{(SRR4)}$$

$$*Li_2S_2 \rightarrow *Li_2S + (1/8)S_8 \qquad \text{(SRR5)}$$

Herein (*) denotes an active site on the g-$C_3N_4$ and g-$C_3N_4$-CNT composite surfaces. For each state of SRR, the reaction Gibbs free energy can be given by equation (1).
Further, the variation in Gibbs free energy at each electrochemical stage of the SRR can be described by the following equations:

$$\Delta G_1 = \left(E_{*S_8} + ZPE_{*S_8} - TS_{*S_8}\right) + 2.(E_{Li} + ZPE_{Li} + TS_{Li}) - \left(E_{*Li_2S_8} + ZPE_{*Li_2S_8} - TZ_{*Li_2S_8}\right),$$

$$\Delta G_2 = \left(E_{*Li_2S_6} + ZPE_{*Li_2S_6} - TZ_{*Li_2S_6}\right) - \left(\frac{1}{4}\right)\left(E_{*S_8} + ZPE_{*S_8} - TS_{*S_8}\right) - \left(E_{*Li_2S_8} + ZPE_{*Li_2S_8} - TZ_{*Li_2S_8}\right),$$

$$\Delta G_3 = \left(E_{*Li_2S_4} + ZPE_{*Li_2S_4} - TZ_{*Li_2S_4}\right) - \left(\frac{1}{4}\right)\left(E_{*S_8} + ZPE_{*S_8} - TS_{*S_8}\right) - \left(E_{*Li_2S_6} + ZPE_{*Li_2S_6} - TZ_{*Li_2S_6}\right),$$

$$\Delta G_4 = \left(E_{*Li_2S_2} + ZPE_{*Li_2S_2} - TZ_{*Li_2S_2}\right) - \left(\frac{1}{4}\right)\left(E_{*S_8} + ZPE_{*S_8} - TS_{*S_8}\right) - \left(E_{*Li_2S_4} + ZPE_{*Li_2S_4} - TZ_{*Li_2S_4}\right),$$

$$\Delta G_5 = \left(E_{*Li_2S} + ZPE_{*Li_2S} - TZ_{*Li_2S}\right) - \left(\frac{1}{8}\right)\left(E_{*S_8} + ZPE_{*S_8} - TS_{*S_8}\right) - \left(E_{*Li_2S_2} + ZPE_{*Li_2S_2} - TZ_{*Li_2S_2}\right),$$

**Table S1:** DFT calculated bandgap and binding energy values (in eV) for $S_8$/LiPSs when adsorbed onto the g-$C_3N_4$ and g-$C_3N_4$-CNT composite surfaces.

| System | Bandgap (eV) | $E_b$ (eV) | System | Bandgap (eV) | $E_b$ (eV) |
|---|---|---|---|---|---|
| **g-$C_3N_4$** | 1.195 | - | **g-$C_3N_4$-CNT** | 0.049 | - |
| **$Li_2S$** | 1.732 | 8.309 | **$Li_2S$** | 0.015 | 1.618 |
| **$Li_2S_2$** | 0.038 | 5.259 | **$Li_2S_2$** | 0.035 | 0.707 |
| **$Li_2S_4$** | 0.008 | 4.352 | **$Li_2S_4$** | 0.015 | 1.776 |
| **$Li_2S_6$** | 0.373 | 3.881 | **$Li_2S_6$** | 0.012 | 2.496 |
| **$Li_2S_8$** | 0.180 | 4.299 | **$Li_2S_8$** | 0.008 | 2.682 |
| **$S_8$** | 1.916 | 2.893 | **$S_8$** | 0.018 | 1.486 |

**Table S2**: Relative energy (in eV) for all possible configurations are considered for $S_8$/LiPSs when adsorbed onto the g-$C_3N_4$ surface.

| System | A | B | C | D | E | F | G | H | I | J | K | L | M | N | O | P | Q |
|---|---|---|---|---|---|---|---|---|---|---|---|---|---|---|---|---|---|
| **$S_8$** | **0** | 0.152 | 0.533 | 0.266 | 0.284 | 0.334 | 0.199 | 0.848 | 0.349 | 0.313 | 0.347 | NA | NA | NA | NA | NA | NA |
| **$Li_2S_8$** | 1.085 | 0.261 | 0.433 | 1.048 | 1.169 | 0.198 | **0** | 0.594 | 0.282 | 0.421 | 0.257 | 0.254 | 1.653 | 1.672 | 1.677 | 1.666 | 1.53 |
| **$Li_2S_6$** | **0** | 0.199 | 0.2 | 0.059 | 0.605 | 0.375 | 0.034 | 0.19 | 0.193 | 0.189 | 0.112 | 1.218 | 0.192 | 0.038 | NA | NA | NA |
| **$Li_2S_4$** | 0.407 | 0.581 | 0.587 | **0** | 0.408 | 0.675 | 0.579 | 0.571 | 0.45 | 0.317 | 0.356 | 0.543 | 0.309 | 0.3052 | 0.405 | 0.304 | NA |
| **$Li_2S_2$** | 1.09 | **0** | 0.286 | 0.906 | 0.285 | 1.481 | 0.403 | 1.071 | 1.31 | 1.006 | 1.007 | 0.983 | 1.007 | 0.983 | NA | NA | NA |
| **$Li_2S$** | 0.115 | 1.146 | 0.237 | 3.566 | 3.425 | 3.425 | 3.541 | **0** | 4.34 | 3.566 | 3.566 | NA | NA | NA | NA | NA | NA |

**Table S3**: Relative energy (in eV) for all possible configurations are considered for $S_8$/LiPSs when adsorbed onto the g-$C_3N_4$-CNT composite surfaces.

| System | A | B | C | D | E | F | G |
|---|---|---|---|---|---|---|---|
| **$S_8$** | **0** | 0.023 | 0.003 | 0.243 | 0.164 | 0.24 | 0.24 |
| **$Li_2S_8$** | 1.115 | 0.376 | **0** | 0.013 | 0.024 | 0.009 | NA |
| **$Li_2S_6$** | 1.087 | 1.089 | 0.211 | 0.993 | 0.94 | **0** | NA |
| **$Li_2S_4$** | 0.072 | 0.055 | 0.048 | 0.032 | **0** | 0.026 | NA |
| **$Li_2S_2$** | 0.086 | 0.093 | 0.099 | **0** | 0.002 | 0.006 | NA |
| **$Li_2S$** | 0.157 | 0.164 | 0.161 | 0.162 | 0.161 | 0.045 | **0** |

**Theoretical calculations:**

**Binding Energy of LiPSs on g-$C_3N_4$ and g-$C_3N_4$-CNT:** We used DFT calculations to explore the binding strength, particularly the absorption characteristics, of S8/LiPSs (Lithium polysulfides) on both g-$C_3N_4$ and g-$C_3N_4$-CNT composite surfaces. Our computed binding energies are consistent with previous investigations conducted on g-$C_3N_4$ surfaces.[1] Upon closer examination of the g-$C_3N_4$/LiPSs interaction (Figure 4a), it becomes evident that the predominant interactions stem from chemical bonds between Li+ ions and the two-fold coordinated nitrogen atoms. This observation underscores the significant role of atomic under-coordination in g-$C_3N_4$ in stabilizing LiPS. Conversely, in the case of g-$C_3N_4$-CNT (see Figure 4b), where all carbon atoms are three-fold coordinated within the carbon nanotube, the absence of chemical bonds between LiPSs and the surface is apparent. This difference in interaction mechanisms may explain why S8/LiPSs exhibit weaker binding affinity on g-$C_3N_4$-CNT compared to g-$C_3N_4$ surfaces. However, to the best of our knowledge, no theoretical reports have yet examined the interaction of LiPSs with g-$C_3N_4$-CNT surfaces. Our experimental results show that LiPSs bind strongly with the g-$C_3N_4$ component of the g-$C_3N_4$-CNT composite surface instead of the CNT.

Through our investigation, we thoroughly explored various potential adsorption sites on the CNTs of g-$C_3N_4$-CNT composites (refer to **Table S2-S3**) and discovered that S8/LiPSs preferentially bind to the CNTs (refer to **Figure 4d**) rather than the g-$C_3N_4$ component of the g-$C_3N_4$/CNT composite This observation suggests that the calculated binding energy values are weaker than those observed for g-$C_3N_4$ alone. This finding agrees with a previous study by Yu et al.[2] where researchers focused on isolated CNT surfaces rather than composite surfaces.

Furthermore, the binding of LiPSs with the CNT component of the g-$C_3N_4$-CNT composite may be attributed to the limitations of conventional geometry optimization methods, which may not fully elucidate the intercalation processes occurring on either the g-$C_3N_4$ or CNT components of the composite surface. We believe that molecular dynamics (MD) simulations might provide more details on the intercalation of LiPSs on the g-$C_3N_4$-CNT composite surface. Molecular dynamics simulations like AIMD explicitly incorporate thermal fluctuations, allowing molecules to explore various conformations and facilitating bond-breaking events. In contrast, normal optimizations freeze the system at a minimum energy configuration without considering thermal effects, potentially hindering the observation of bond dissociation events that require additional energy. Also, the dynamic representation provided by AIMD simulations, with thermal fluctuations accounted for, enables the observation of bond-breaking events that may not be accessible in static optimizations, where the system remains frozen at a minimum energy state.

**Gibbs Free Energy vs Binding Energy:** In general, effective catalysts facilitate the conversion of LiPSs with minimal changes in free energy, except during the phase transition from liquid to solid. However, the data for g-$C_3N_4$ and g-$C_3N_4$-CNT molecules show significant free energy changes during the conversion of $Li_2S_8$ to $Li_2S_4$, which suggests that these materials may not be acting as typical catalysts in this context. The literature suggests that effective catalysts should suppress the shuttle effect by facilitating the conversion of LiPSs. [3–6] If the g-$C_3N_4$ and g-$C_3N_4$-CNT systems are not adequately suppressing this effect, it could lead to inefficient conversion and higher free energy values.

The g-$C_3N_4$ and g-$C_3N_4$-CNT systems may have different catalytic activities compared to the materials commonly reported. This could be due to the unique electronic structure or surface properties of these materials, which affect the interaction with LiPSs. This is evident from the calculated electronic bandgap (**Table S1**) of the g-$C_3N_4$ and g-$C_3N_4$-CNT in the presence of LiPSs which shows countable changes in the bandgap properties of these materials. The binding energy data indicates that both systems have a strong interaction with LiPSs, particularly in the case of $Li_2S_8$ and $Li_2S_6$. This strong binding could lead to a higher energy barrier for the conversion process, resulting in the observed increase in free energy. Further, the presence of CNT in the g-$C_3N_4$-CNT system has altered the electronic properties (bandgap lowered from 1.195 eV to 0.049 eV) and, consequently, the catalytic behavior. This could explain why the free energy changes are less pronounced in the g-$C_3N_4$-CNT system compared to the g-$C_3N_4$ system alone.

Further, examining the Gibbs free energy values for different LiPS species in both systems—g-$C_3N_4$ with individual molecules and g-$C_3N_4$ incorporated into CNTs (g-$C_3N_4$-CNT) with individual molecules—we observe a pronounced increase in free energy from $Li_2S_8$ to $Li_2S_6$ and then to $Li_2S_4$, indicating an uphill process. This deviation from the expected behavior in other effective catalysts suggests energetically unfavorable transformations between these polysulfide components. Correlating this with the binding energy data reveals insightful patterns. Binding energy values generally increase as the number of lithium atoms in the polysulfide species decreases. In both systems, $Li_2S$ exhibits the highest binding energy, followed by $Li_2S_8$, $Li_2S_6$, $Li_2S_4$, $Li_2S_2$, and $S_8$. This suggests that $Li_2S$ forms the strongest interaction with the respective catalytic surface, while $S_8$ shows the weakest interaction.

Comparing the binding energy values between the two systems highlights a trend: the presence of CNTs generally leads to lower binding energy values for most sulfur species. This implies weaker interactions between the polysulfides and the catalytic surface when CNTs are present, potentially contributing to the observed increase in free energy during the transformation of lithium polysulfide components.

Therefore, the discrepancy observed in **Figure 4d** may be attributed to the interplay between the energetics of the chemical transformations (as reflected in the Gibbs free energy) and the strength of interactions between the polysulfide species and the catalytic surfaces (as indicated by the binding energy). The weakening of these interactions in the presence of CNTs could lead to energetically unfavorable transformations, resulting in the observed uphill process. This underscores the complexity of surface interactions in catalytic systems and emphasizes the importance of considering both thermodynamics and surface chemistry in understanding catalytic processes.

**Table S4:** Comparison of Li-S battery performance with previously published works.

| Host material | Specific surface area ($m^2/g$) | Sulfur content (%) | Initial capacity (mAh/g) | Retained capacity (mAh/g) | Rate | Cycle number | Cell format | Ref |
|---|---|---|---|---|---|---|---|---|
| g-$C_3N_4$ nanosheets | 209 | 70.4 | 960 | 578 | 0.1 C | 750 | Coin | [7] |
| g-$C_3N_4$ spheres | 931 | 69.8 | 934 | 775 | 0.5 C | 100 | Coin | [8] |
| Porous g-$C_3N_4$ | 83 | 68.67 | 734 | 620 | 1 C | 300 | Coin | [9] |
| g-$C_3N_4$/C porous cages | 428 | 67 | 1240 | 729 | 1 C | 200 | Coin | [10] |
| Hierarchically porous g-$C_3N_4$/C | 498 | 64.5 | 1150 | 1128 | 0.2 C | 100 | Coin | [11] |
| 3D porous g-$C_3N_4$/ graphene sponge | 827 | 731 | 1132 | 974 | 0.2 C | 800 | Coin | [12] |
| 3D porous g-$C_3N_4$/ CNT | 202 | 80 | 1023 | 583 | 1 C | 500 | Coin | [13] |
| 3D g-$C_3N_4$/rGO/CNT microspheres | 225 | 70.8 | 730 | 620 | 1 C | 500 | Coin | [14] |
| **g-$C_3N_4$ + CNT** | **49** | **68.6** | **895** | **756** | **0.1 C** | **250** | Pouch | This work |

**Table S5:** Results obtained from Nyquist plot for fresh and cycled cells.

| Electrode | Condition | $R_e$ | $R_{ct}$ |
|---|---|---|---|
| g-$C_3N_4$-CNT/S | Fresh cell | 2.7 | 22.6 |
| | After 250 cycles | 5.2 | 14.4 |
| g-$C_3N_4$/S | Fresh cell | 4.2 | 35.6 |
| | After 110 cycles | 11.1 | 16.1 |

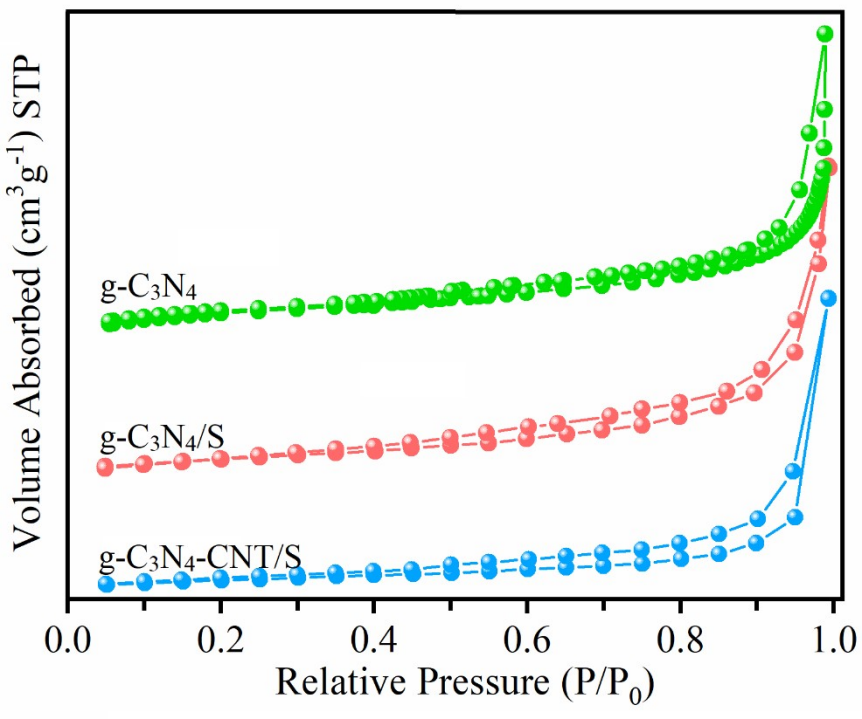


**Figure S1:** $N_2$ sorption isotherms for the prepared materials.

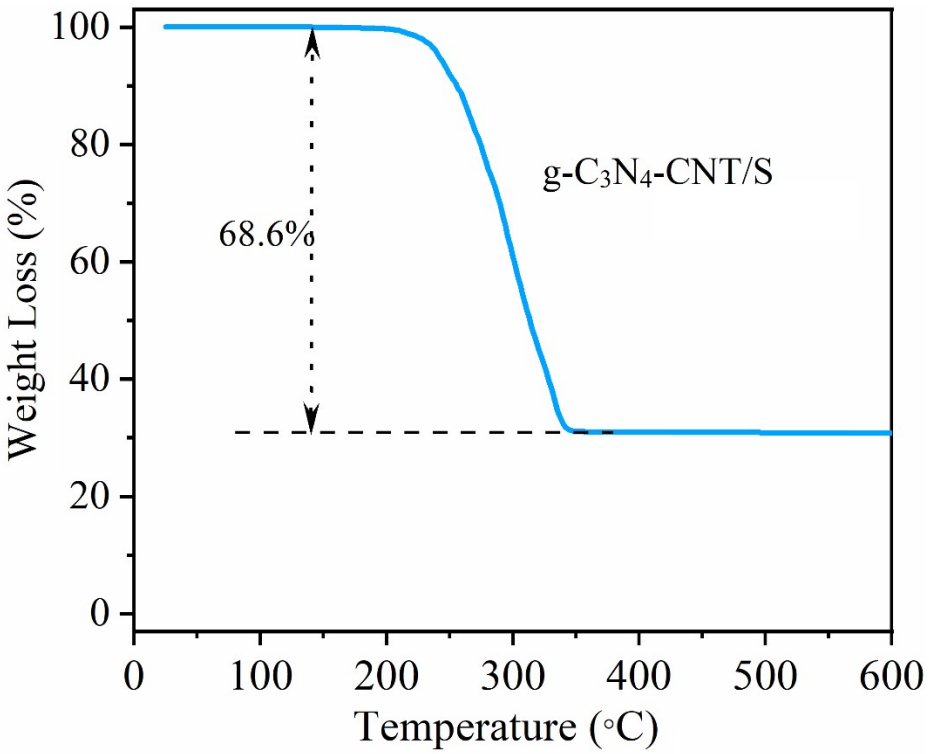


**Figure S2:** TGA profile of g-$C_3N_4$-CNT/S composite confirming the presence of 68.6 wt% sulfur.

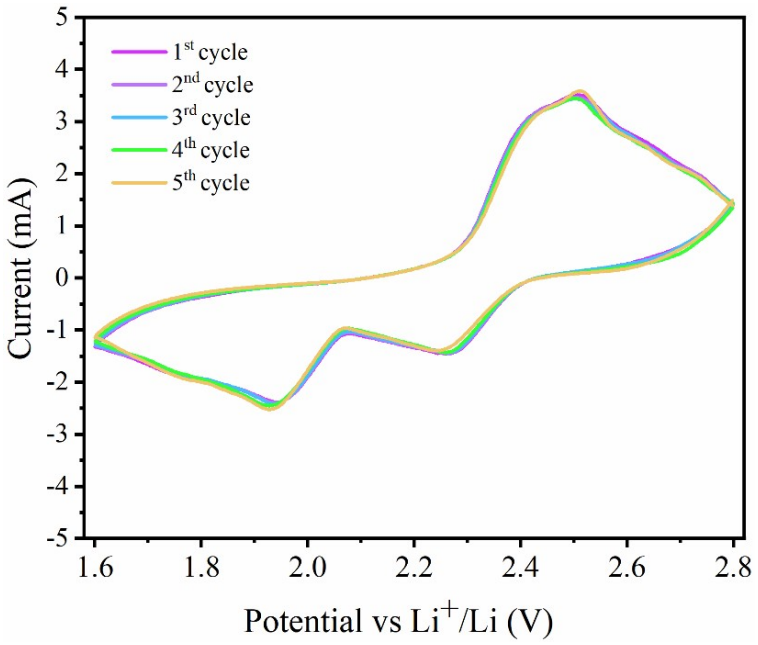


**Figure S3:** CV curves of the g-$C_3N_4$-CNT/S cathode for 5 consecutive cycles.

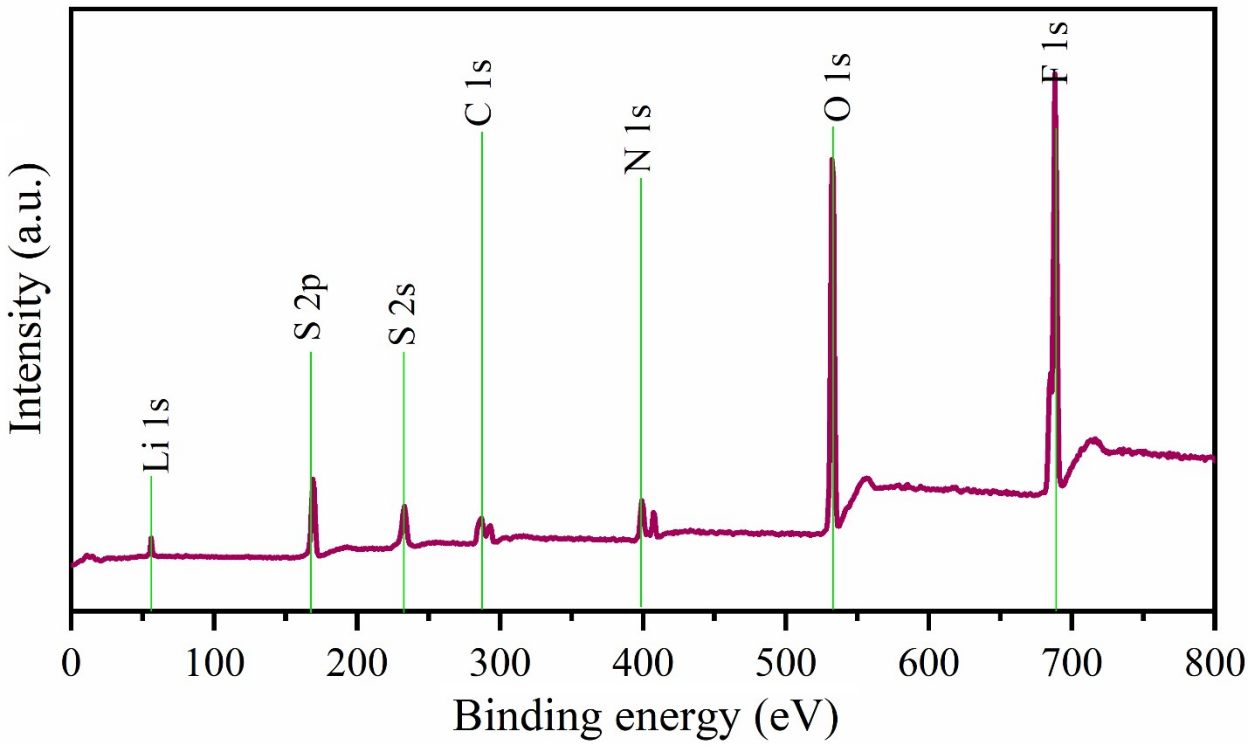


**Figure S4:** Complete XPS scan spectrum of the g-$C_3N_4$-CNT/S cathode obtained from the pouch cell cycled for 250 charge-discharge cycles.

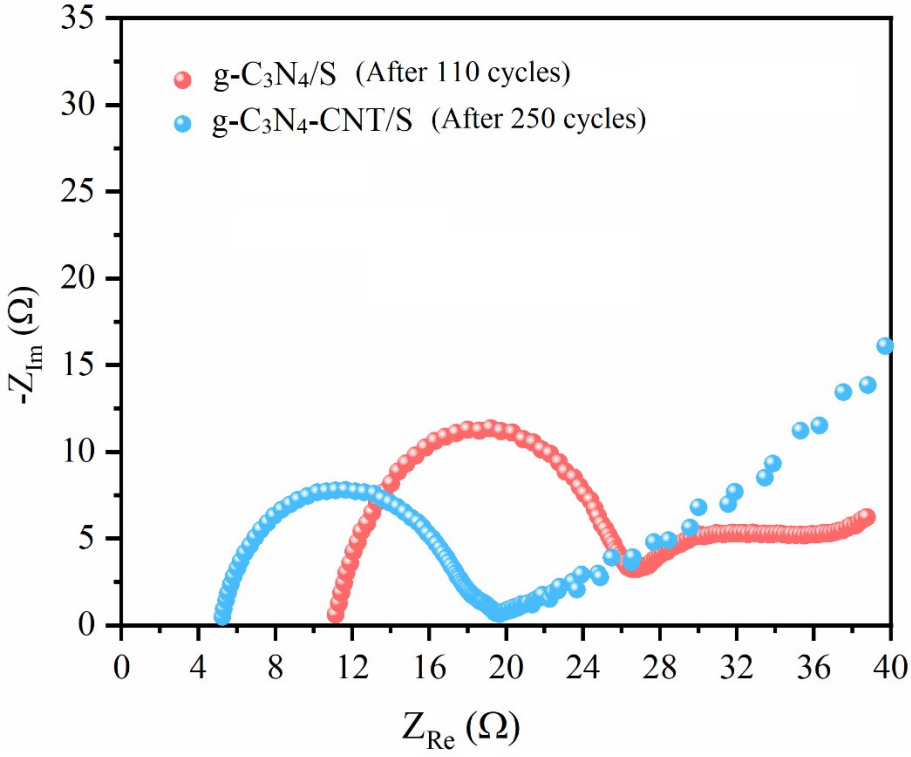


**Figure S5:** EIS spectra of g-$C_3N_4$-CNT/S cathode extracted from the pouch cell after 250 charge-discharge cycles.

## References:


1 K. Liao, P. Mao, N. Li, M. Han, J. Yi, P. He, Y. Sun and H. Zhou, *J Mater Chem A Mater*, 2016, **4**, 5406–5409.

2 B. Yu, A. Huang, D. Chen, K. Srinivas, X. Zhang, X. Wang, B. Wang, F. Ma, C. Liu, W. Zhang, J. He, Z. Wang and Y. Chen, *Small*, 2021, **17**, 2100460.

3 J. Wang, L. Wang, Z. Li, J. Bi, Q. Shi and H. Song, *Journal of Electronic Materials 2023 52:6*, 2023, **52**, 3526–3548.

4 Y. Li, Y. Liu, J. Zhang, D. Wang and J. Xu, *Nanomaterials*, 2024, **14**, 692.

5 D. He, C. Zhu, Y. Huo and Z. Rao, *J Mater Sci Technol*, 2024, **169**, 105–114.

6 X. Liu, Y. Zheng, M. Zhang, S. Qi, M. Tan, R. Zhao and M. Zhao, *Adv Mater Interfaces*, 2023, **10**, 2202205.

7 Z. Meng, Y. Xie, T. Cai, Z. Sun, K. Jiang and W. Q. Han, *Electrochim Acta*, 2016, **210**, 829–836.

8 Z. Meng, S. Li, H. Ying, X. Xu, X. Zhu and W. Q. Han, *Adv Mater Interfaces*, 2017, **4**, 1601195.

9 D. Li, J. Liu, W. Wang, S. Li, G. Yang, P. Wang, K. Zhu and Z. Li, *Appl Surf Sci*, 2021, **569**, 151058.

10 P. Song, Z. Chen, Y. Chen, Q. Ma, X. Xia and H. Liu, *Electrochim Acta*, 2020, **363**, 137217.

11 X. Hong, Y. Liu, J. Fu, X. Wang, T. Zhang, S. Wang, F. Hou and J. Liang, *Carbon N Y*, 2020, **170**, 119–126.

12 J. Zhang, J. Y. Li, W. P. Wang, X. H. Zhang, X. H. Tan, W. G. Chu and Y. G. Guo, *Adv Energy Mater*, 2018, **8**, 1702839.

13 W. He, X. He, M. Du, S. Bie, J. Liu, Y. Wang, M. Liu, Z. Zou, W. Yan and H. Zhao, *Journal of Physical Chemistry C*, 2019, **123**, 15924–15934.

14 J. Wang, Z. Meng, W. Yang, X. Yan, R. Guo and W. Q. Han, *ACS Appl Mater Interfaces*, 2019, **11**, 819–827.